Roaming in the Unimolecular Decay of *syn*-Methyl-Substituted Criegee Intermediates

Tianlin Liu and Marsha I. Lester*
Department of Chemistry, University of Pennsylvania,
Philadelphia, PA 19104-6323, USA

Abstract

Alkene ozonolysis generates transient carbonyl oxide species, known as Criegee intermediates, which are a significant non-photolytic source of OH radicals in the troposphere. This study demonstrates that unimolecular decay of *syn*-methyl-substituted Criegee intermediates proceeds via 1,4 H-atom transfer to vinyl hydroperoxides, resulting in O–O fission to OH products or, alternatively, OH roaming to hydroxycarbonyl products. Newly generated Criegee intermediates are shown to yield hydroxycarbonyls with sufficient internal excitation to dissociate via C–C fission to acyl and hydroxymethyl (CH_2OH) radicals. The stabilized Criegee intermediates and unimolecular products are rapidly cooled in a pulsed supersonic expansion for photoionization detection with time-of-flight mass spectrometry. CH_2OH products are identified by 2+1 resonance-enhanced multiphoton ionization via the $3p_z$ Rydberg state upon unimolecular decay of CH_3CHOO, $(CH_3)_2COO$, $(CH_3)(CH_3CH_2)COO$, and $(CH_3)(CH_2{=}CH)COO$ (methyl vinyl ketone oxide). The stabilized Criegee intermediates are separately detected using 10.5 eV photoionization. This study provides the first experimental evidence of roaming in the unimolecular decay of isoprene-derived methyl vinyl ketone oxide, and extends earlier studies that reported stabilized hydroxycarbonyl products.

* Corresponding author email: milester@sas.upenn.edu

Introduction

The hydroxyl (OH) radical is a key atmospheric oxidizing agent, which initiates the oxidative breakdown of most volatile organic compounds (VOC) emitted into the troposphere.[1, 2] Solar photolysis of tropospheric ozone and subsequent reaction of O (^{1}D) products with water vapor is the primary source of OH radicals.[1, 2] Ozonolysis of alkenes, generally derived from abundant biogenic VOC sources such as isoprene, provides an alternative non-photolytic source of tropospheric OH radicals in the daytime, particularly in wintertime, and is the source of OH radicals at nighttime.[3-6]

Alkene ozonolysis proceeds by 1,3-dipolar cycloaddition of ozone across a C=C double bond, transiently forming a cyclic primary ozonide (POZ). The POZ rapidly decomposes to carbonyl and zwitterionic carbonyl oxide [RR′C=O$^+$O$^-$] products, the latter known as Criegee intermediates.[7, 8] The nascent and thermalized Criegee intermediates can undergo unimolecular decay to OH radicals,[9] thereby contributing to the oxidative capacity of the atmosphere.[6, 10] Alternatively, bimolecular reactions of the stabilized Criegee intermediates with other atmospheric species, including water vapor, SO_2, and acids, can lead to functionalized hydroperoxides and aerosol precursors.[11, 12]

For Criegee intermediates with a methyl group oriented towards the carbonyl oxide group (*syn*-methyl-substituted Criegee intermediates, *syn*-CH_3RCOO with R = H, CH_3, CH_2CH_3, and $CH{=}CH_2$), unimolecular decay generally occurs by 1,4 H-atom transfer from the methyl substituent to the terminal O-atom as shown in Scheme 1 and Figure 1. The reaction proceeds through a five-membered cyclic transition state (TS) with a barrier of 16–18 kcal mol^{-1}.[9, 11, 13-20] The Criegee intermediates can surmount or tunnel through the TS barrier to form vinyl hydroperoxide (VHP) intermediates, which generally decay by prompt O–O cleavage to form OH and vinoxy radical products.

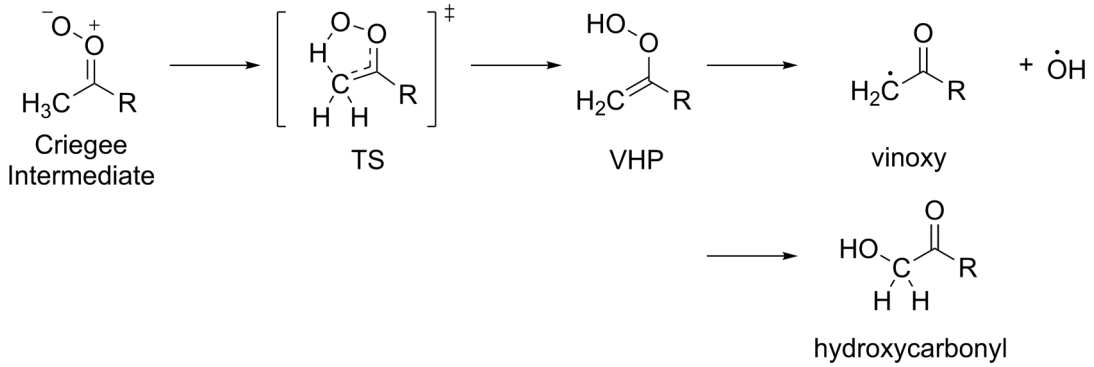

Scheme 1. The conventional 1,4 H-atom transfer mechanism for unimolecular decay of methyl-substituted Criegee intermediates yields vinoxy + OH radical products. Alternatively, the separating OH radical can roam and lead to hydroxycarbonyl products. In this work, R = H, CH_3, CH_2CH_3, and $CH{=}CH_2$.

Recent theoretical investigations have examined alternative pathways for unimolecular decay of Criegee intermediates following 1,4 H-atom transfer to VHPs.[19, 21-24] A recent exploration considered the

possibility of classical OH migration via a ca. 20 kcal mol^{-1} barrier leading to hydroxyacetone.[21] Subsequent theoretical analyses have identified a more favorable low energy pathway, termed "roaming", leading to hydroxycarbonyl products from several Criegee intermediates.[19, 22-24] Roaming involves O–O bond elongation, leading to long range regions of the potential where the separating OH radical can reorient, roam, and add to the CH_2 group of the vinoxy radical, resulting in roaming-induced isomerization to hydroxycarbonyl products. The resultant hydroxycarbonyl products are remarkably stable isomers (ca. –90 kcal mol^{-1}) of the Criegee intermediates (Scheme 1 and Figure 1).[19, 22-24] Under thermalized and atmospheric conditions, hydroxycarbonyl products of roaming will be collisionally stabilized in their deep potential well.

However, under collision-free or limited collision conditions, the initially energized hydroxycarbonyl formed via roaming will likely dissociate via C–C bond fission to different radical products.[19] For example, C–C fission can lead to hydroxymethyl [CH_2OH] and acyl [RC(O)] radical products, as shown in Scheme 2, which lie lower in energy than the OH + vinoxy radical asymptote from O–O fission.[19, 23] The OH group of the CH_2OH product is indicative of the 1,4 H-atom transfer step, while the C–OH bond reflects OH addition to the CH_2 group as a result of roaming.

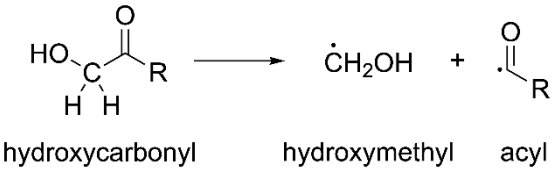

Scheme 2. C–C fission of hydroxycarbonyl yields hydroxymethyl and acyl radicals.

An overview of the unimolecular reaction pathways leading from *syn*-methyl-substituted Criegee intermediates to OH + vinoxy, hydroxycarbonyl, and/or hydroxymethyl + acyl products is illustrated in Figure 1. The representative energies are for unimolecular decay of an isoprene-derived Criegee intermediate, methyl vinyl ketone oxide [$(CH_3)(CH_2{=}CH)COO$, *trans*-MVK-oxide], reported previously in Ref. 19. The computed pathways for the four distinct Criegee intermediate (CI) systems investigated in this work (R = H, CH_3, CH_2CH_3, and $CH{=}CH_2$) are similar as shown in Figure S1.

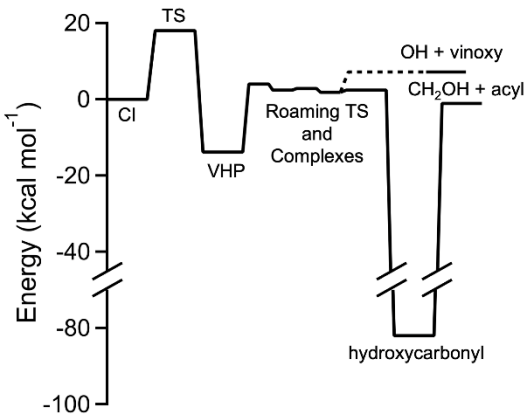

Figure 1. Schematic reaction pathway for unimolecular decay of *syn*-methyl-substituted Criegee intermediates (CI). Unimolecular decay proceeds via a transition state (TS) associated with 1,4 H-atom transfer to form a vinyl hydroperoxide (VHP) intermediate, followed by O–O fission to release OH + vinoxy radicals (dashed) or roaming of the separating OH and vinoxy radicals to form hydroxycarbonyl. C–C fission of the hydroxycarbonyl leads to CH_2OH + acyl radicals. Representative energies are for unimolecular decay of *syn*-MVK-oxide and are adapted with permission from Ref. 19. Copyright 2018 American Chemical Society. Analogous unimolecular reaction pathways have been predicted for other CIs as shown in Figure S1.

Early ozonolysis studies on tetramethylethylene reported hydroxyacetone [$HOCH_2C(O)CH_3$] as a stable end product utilizing Fourier-transform infrared spectroscopy (FTIR)[25] and liquid chromatography.[26] Other hydroxycarbonyls have been observed in more recent studies of alkene ozonolysis. Specifically, glycolaldehyde [$HOCH_2CHO$] was identified as a product from ozonolysis of *trans*-2-butene in a jet-stirred reactor coupled with tunable vacuum ultraviolet (VUV) photoionization and mass spectrometric detection.[27] In addition, 2-hydroxypropanal [$CH_3CH(OH)CHO$] was observed by FTIR as a decay product following ozonolysis of *cis*-2-penten-1-ol in an Atmospheric Simulation Chamber.[28]

Since 2012, Criegee intermediates with various substituents have been generated using an alternative synthetic method involving photolysis of diiodo-alkane or -alkene precursors and subsequent reaction with oxygen.[19, 29] In 2017, hydroxyacetone was identified as an isomeric product of the dimethyl-substituted Criegee intermediate, $(CH_3)_2COO$, under thermal flow cell conditions (10 Torr, 298 K).[21] Recently, hydroxybutanone [$CH_3CH_2C(O)CH_2OH$ and/or $CH_3CH(OH)C(O)CH_3$][23] was observed with a kinetic time profile of appearance that matched the experimental thermal unimolecular decay rate of the methyl-ethyl-substituted Criegee intermediate [$(CH_3)(CH_3CH_2)COO$, MECI] under thermal flow cell conditions (10 Torr, 298 K). In both cases, the hydroxycarbonyls were distinguished from the parent Criegee intermediates with the same mass by their distinctive photoionization thresholds and spectra utilizing tunable VUV synchrotron radiation. Additionally, the kinetic time profiles of the

hydroxycarbonyls were characteristic of stable molecules with persistent photoionization signals at long time.

In this laboratory, CH_3CHOO,[15, 30, 31] $(CH_3)_2COO$,[14, 32] MECI,[18, 33] and methyl vinyl ketone oxide [$(CH_3)(CH_2{=}CH)COO$, MVK-oxide][19, 34] have been generated by photolysis of diiodo precursors in an O_2/Ar carrier gas within a quartz capillary reactor tube prior to cooling in a supersonic free jet expansion. In each case, a portion of the newly formed Criegee intermediates undergoes unimolecular decay within the reactor tube, yielding OH radicals that are cooled in the supersonic expansion and have been detected by UV laser-induced fluorescence (LIF) on OH A-X (1,0) transitions.[14, 17, 18, 30] (In IR action spectra of Criegee intermediates, OH radicals released in the source are considered as 'background OH' and removed using an active background subtraction technique.[13, 15, 18, 19, 30]) Later, vinoxy and 1-methyl vinoxy radicals resulting from unimolecular decay of CH_3CHOO and $(CH_3)_2COO$, respectively, within the capillary tube were similarly cooled in the supersonic expansion and detected by LIF on B-X transitions.[35]

In the present study, we observe CH_2OH radicals generated upon unimolecular decay of several Criegee intermediates within the reactor tube, which are cooled in the supersonic expansion and detected by 2+1 REMPI. In prior laboratory studies, CH_2OH radicals were generated by the reaction of chlorine or fluorine atoms with methanol.[36, 37] The resultant CH_2OH radicals were efficiently detected via 2+1 REMPI using visible light between 425–495 nm with ion signals detected on the parent mass, m/z 31. The REMPI spectrum of CH_2OH was first reported by Dulcey and Hudgens[37] using a discharge flow reactor at a pressure of 2 Torr. Aristov et al. later produced CH_2OH in a molecular beam and reported a jet-cooled REMPI spectrum, which resolved rotational band structure and reported an excited state lifetime of 0.5 ± 0.1 ps.[38] The excited state involved in the two-photon electronic transition was attributed to a $3p_z$ Rydberg state based on a molecular orbital symmetry analysis.[38] The REMPI spectrum of CH_2OH is vibrationally resolved, and provides information about vibrational modes in the $3p_z$ Rydberg state.

The structures and energies of CH_2OH in the ground and excited electronic states of the neutral and cation have been extensively investigated using various theoretical methods.[39-45] The CH_2OH radical can be treated as a planar molecule of C_s symmetry. The ground state singly occupied molecular orbital (SOMO) contains the unpaired electron in a π^* orbital with a node on the CO bond. The lowest four excited states have been classified as $3s$, $3p_x$, $3p_y$, $3p_z$ Rydberg states, and the vertical and adiabatic excitation energies have been computed with different multireference methods.[39, 44, 45] The cationic state of CH_2OH belongs to the C_s point group,[41] which has increased π bond character upon removal of an electron from the antibonding SOMO.

In this work, we observe CH_2OH radicals resulting from C–C fission of hydroxycarbonyls. The hydroxycarbonyls are generated by OH roaming in the unimolecular decay of several *syn*-methyl-substituted Criegee intermediates. Four Criegee intermediates are investigated, CH_3CHOO, $(CH_3)_2COO$, MECI, and MVK-oxide, each of which has one or more conformers that decay via a 1,4 H-atom transfer mechanism to produce vinyl hydroperoxide intermediates [CH_2=C(OOH)R], followed by OH roaming that yields hydroxycarbonyls [$HOCH_2C(O)R$] and its CH_2OH and acyl fragments. In each case, CH_2OH radicals are identified by vibrationally-resolved 2+1 REMPI spectra on the $3p_z \leftarrow\leftarrow \pi^*$ electronic transition. The experimental results are combined with high-level multireference calculations in order to characterize the electronic transition energies of CH_2OH radicals.

Methods

The generation of Criegee intermediates from diiodo-precursors has been described previously.[18, 31-33] Briefly, the precursors are heated to 50 °C (vapor pressures in Table S1), and the vapor is entrained in 20% O_2/Ar carrier gas mixture (4 psig) and pulsed through a nozzle (Parker-Hannifin General Valve Series 9, 1 mm orifice) into a quartz capillary tube reactor (1 mm ID, 25 mm length) at 10 Hz. The pressure and temperature is expected to be uniform as the gas passes through the capillary reactor tube based on Poiseuille's law for viscous flow through a cylindrical tube.[46, 47] The precursors are photolyzed by 248 nm radiation from a KrF excimer laser (Coherent, Compex 102, 10 Hz) which is cylindrically focused along the capillary reactor tube. The 248 nm photolysis results in C–I bond breakage, generating monoiodo-alkyl or -alkenyl radicals that subsequently react with O_2 to produce Criegee intermediates.

The Criegee intermediates are generated with sufficient internal excitation for some to undergo unimolecular decay prior to collisional stabilization within the capillary reactor tube. The stabilized Criegee intermediates, products of unimolecular decay, and other components in the gas mixture are cooled to a low rotational temperature (ca. 10 K) in the supersonic expansion.

Approximately 4.5 cm (ca. 80 μs) downstream from the exit of the capillary, the gas mixture is intersected by a photoionization laser beam in the collision-free region, and the cations are detected using a time-of-flight mass spectrometer (TOF-MS). Two photoionization methods are utilized. The first utilizes VUV radiation at 118 nm (10.5 eV), generated by frequency tripling the third harmonic output (ca. 35 mJ pulse^{-1}) of a Nd:YAG laser (Continuum Powerlite 9010, 10 Hz) in a phase-matched Xe: Ar gas mixture. The second photoionization laser source is visible radiation (450–500 nm, ca. 13 mJ pulse^{-1}, 40 cm focal length lens) from a broadly tunable β-barium borate optical parametric oscillator (BBO-OPO, EKSPLA 342NT, 3–5 ns pulse width, 4.7 cm^{-1} linewidth at 490 nm, 10 Hz). The visible light is utilized to selectively ionize CH_2OH radicals by 2+1 REMPI.[38] The frequencies (vacuum) of the BBO-OPO output are calibrated using a wavemeter (Coherent WaveMaster).

Theoretically, geometry optimization and harmonic frequency calculations are carried out for the ground and excited electronic (Rydberg *3p*) states of CH_2OH using complete Active Space Second Order Perturbation Theory (CASPT2) coupled to Dunning's augmented basis sets (aug-cc-pVXZ, X = D, T, Q) as implemented in MOLPRO v2020.1.[48, 49] The CASPT2 calculations are based on five-doublet state-averaged Complete Active Space Self-Consistent Field (SA5-CASSCF) reference wavefunctions involving an active space of 3 electrons in 6 orbitals. The orbitals in the active space consist of π and π* orbitals, and *3s*, $3p_x$, $3p_y$, $3p_z$ Rydberg orbitals. An imaginary level shift of 0.3 Hartree is applied to the CASPT2 calculations to mitigate the involvement of intruder states and facilitate convergence. The adiabatic excitation energy (AEE) calculations include single-point energy calculations using multireference configuration interaction (MRCI) plus the Davidson correction (MRCI + Q), and the zero-point energy correction obtained at the CASPT2 level. The same active space is used in the MRCI calculations. Geometry optimization and harmonic frequency calculations are also carried out for the ground state CH_2OH and acyl radical coproducts (Table S2) using CCSD(T)/cc-pVTZ level of theory, which is utilized to estimate energy partitioning among the two fragments during C–C fission of hydroxycarbonyls. All calculations are performed using MOLPRO v2020.1 on the ACCESS resources.

Results

A. Experimental results

The present study identifies hydroxymethyl (CH_2OH) radicals derived from OH roaming in the unimolecular decay of four *syn*-methyl-substituted Criegee intermediates. In depth experimental results are initially presented for $(CH_3)_2COO$, which has a single conformational form. The results are then expanded to other Criegee intermediates, which have multiple conformational forms, only some of which can undergo unimolecular decay via a 1,4 H-atom transfer mechanism that can lead to CH_2OH.

$(CH_3)_2COO$ is generated by photolysis of the $(CH_3)_2CI_2$ precursor using 248 nm radiation (ca. 115 kcal mol^{-1}) from an excimer laser, resulting in C–I bond dissociation (ca. 50 kcal mol^{-1}), followed by O_2 addition and displacement of the remaining I-atom. While detailed energetics associated with formation of $(CH_3)_2COO$ have not been reported, prior studies of CH_2OO suggest that ca. 90% of the excess energy from photolysis will be partitioned into the resulting monoiodo radical,[50, 51] followed by near-thermoneutral reaction with O_2.[52-54] Assuming similar energetics for $(CH_3)_2COO$,[35, 50] some portion of the newly formed $(CH_3)_2COO$ will be born with sufficient internal energy (on the order of 50 kcal mol^{-1}) to undergo unimolecular decay (Scheme 1) prior to stabilization in the capillary reactor tube. The ensuing supersonic expansion will then contain collisionally stabilized $(CH_3)_2COO$ Criegee intermediates, OH and 1-methyl vinoxy radicals, potential roaming products (Schemes 1 and 2), and other components of the gas mixture.

The experimental conditions are initially optimized for production of $(CH_3)_2COO$ utilizing VUV photoionization at 10.5 eV (118 nm) on the m/z 74 mass channel, as shown in Figure S2. CH_2OH radicals are detected on the m/z 31 mass channel using 2+1 REMPI via the $3p_z$ Rydberg state of CH_2OH.[38] $(CH_3)_2COO$ and CH_2OH are cooled in the supersonic expansion and detected under collision-free conditions in the TOF-MS. In both cases, the optimal photoionization signal intensities are achieved with very similar 248 nm photolysis conditions (time and position).

The REMPI spectrum of CH_2OH has been extensively mapped previously,[38] and a full analysis is not the goal of this work. Instead, a section of the spectrum is recorded in order to confirm the identity of the CH_2OH product. The experimental 2+1 REMPI spectrum of CH_2OH radical is obtained by scanning the visible output of the BBO-OPO from 450 to 500 nm. The BBO-OPO has a linewidth of ca. 5 cm^{-1} (ca. 0.1 nm), resulting in a two-photon energy resolution of ca. 10 cm^{-1} (ca. 0.2 nm). A rapid scan with step size of 0.1 nm reveals six strong features, as shown in Figure 2 (gray), and subsequent slow scans of each feature are performed with a smaller step size of 0.02 nm (black).

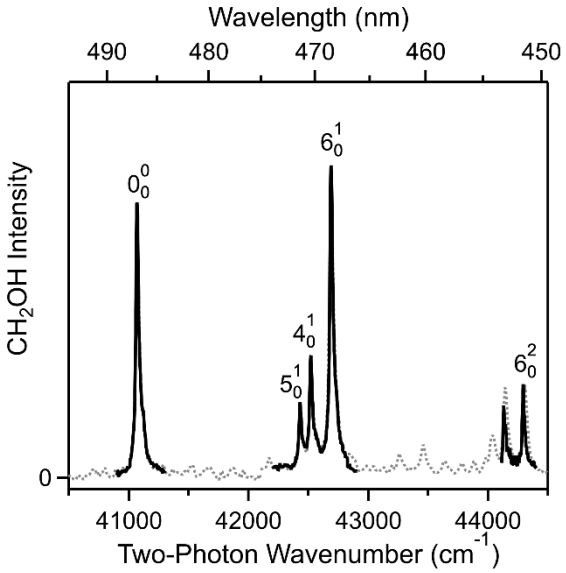

Figure 2. 2+1 REMPI spectrum of CH_2OH radicals observed upon laboratory generation of the $(CH_3)_2COO$ Criegee intermediate in a quartz capillary reactor tube, followed by supersonic expansion. The REMPI spectrum is attributed to the $3p_z \leftarrow\leftarrow \pi^*$ transition of the CH_2OH radical. The CH_2OH radical is produced by C–C fission of hydroxyacetone, which results from OH roaming in the unimolecular decay of $(CH_3)_2COO$. Each segment of the spectrum is a composite of several data sets, smoothed with a 3-point binomial method. The black traces are scanned with step size of 0.02 nm and the gray traces are scanned with a step size of 0.1 nm, corresponding to two-photon energies of 2 and 10 cm^{-1}. The vibronic assignments are adopted from the previously reported spectrum for the CH_2OH in Ref. 38.

The lowest energy feature observed at 487.0 nm (two-photon energy of ca. 41070 cm^{-1}) is consistent with the previously reported value of 41062 cm^{-1} for the electronic origin (0_0^0) of the $3p_z \leftarrow\leftarrow \pi^*$ transition of CH_2OH radicals.[38] Another strong feature observed ca. 1620 cm^{-1} to higher energy agrees

with a previously report of the ν_6 CO stretch mode (6_0^1) at 1625 cm^{-1}.[55] An additional feature observed ca. 1600 cm^{-1} to higher energy has been ascribed previously to 6_0^2.[38] These three features form a vibrational progression in the totally symmetric CO stretch mode of the *3p*$_z$ excited state, indicating a large geometry change between the ground and electronic excited states. The feature adjacent to the 6_0^2 feature at ca. 453.2 nm was also observed but not assigned in the previously reported jet-cooled REMPI spectrum of CH_2OH.[38] Other features observed ca. 1450 and 1360 cm^{-1} to higher energy of the origin were previously assigned to 4_0^1 and 5_0^1, involving CH_2 scissor (ν_4) and in-phase HCOH bend (ν_5) modes, respectively.[38] Thus, the two-photon REMPI transitions observed in this work provide definitive identification of CH_2OH products in the unimolecular decay of $(CH_3)_2COO$.

Rotational band contour simulation (Figure S3) of the electronic band origin (0_0^0) reveals a rotational temperature of ca. 10 K for the CH_2OH radical, indicating efficient rotational cooling in the supersonic expansion. However, as shown in Figure S4, a weak feature is observed at 501.4 nm, ca. 1180 cm^{-1} to lower energy of the electronic origin. Based on comparison with the previously reported REMPI spectrum, this feature is ascribed to a vibrational hot band (6_1^0) of the CH_2OH radical, indicating incomplete vibrational cooling in the supersonic expansion. Details are provided in the Supporting Information (SI).

CH_2OH REMPI signals are also observed upon generation of CH_3CHOO, MECI, and MVK-oxide. In each case, stabilized CH_3CHOO, MECI, and MVK-oxide are detected by 10.5 eV VUV photoionization (Figure S2) on m/z 60, m/ 88, and m/z 86, respectively. For each Criegee intermediate, one or more of its lowest energy conformers has a methyl (CH_3) group adjacent to the terminal O, and thus can undergo unimolecular decay via 1,4 H-atom transfer, transiently forming a VHP, followed by O–O bond breakage to yield OH radicals, as observed in prior studies.[14, 18, 19, 56] An alternative OH roaming mechanism will lead from VHP to hydroxycarbonyl products, which are formed with substantial internal energy (Figures 1 and S1). C–C fission of the hydroxycarbonyl molecules prior to collisional stabilization results in CH_2OH + acyl radical products (Scheme 2). Maximum CH_2OH signals are observed under experimental conditions that also optimize VUV photoionization signals of the Criegee intermediates. The structures and names of the species involved in the unimolecular decay of Criegee intermediates are given in Table S2.

The signal intensities of CH_2OH (m/z 31) observed upon unimolecular decay of different Criegee intermediates are measured using 2+1 REMPI on the strongest 6_0^1 band of *3p*$_z$ ←← π* transition at ca. 468.5 nm. The observed 6_0^1 features of CH_2OH radicals originating from different Criegee intermediates show very similar breadth (Figure S5), indicating effective rotational cooling (T_{rot} ~ 10 K) in these parallel measurements. The CH_2OH signals shown in Figure 3 are scaled relative to the separately

measured photoionization signal intensity of the corresponding Criegee intermediate on its mass channel (Figure S2), in order to compare the relative yield of CH_2OH products from different Criegee intermediates. This scaling takes into account many factors, e.g. vapor pressure and absorption cross section (at 248 nm) of the diiodo-precursors, etc., that lead to different yields of Criegee intermediates. The resultant CH_2OH to Criegee intermediate signal ratios provide a qualitative measure of their yields under the present experimental conditions as shown in Figure 3. The CH_2OH signal intensity is largest from $(CH_3)_2COO$, which is ca. 2-fold greater than that from MECI and ca. 7-fold greater than that from CH_3CHOO or MVK-oxide. However, the CH_2OH to Criegee intermediate photoionization intensity ratios will be dependent on many factors, including the conformer distribution of the Criegee intermediates. Many other factors may impact the ratios including the yield of roaming and degree of stabilization of the hydroxycarbonyl product under the present experimental conditions. Nevertheless, the observation of CH_2OH products provides direct experimental evidence of roaming in the unimolecular decay of four *syn*-methyl-substituted Criegee intermediates, including isoprene-derived MVK-oxide.

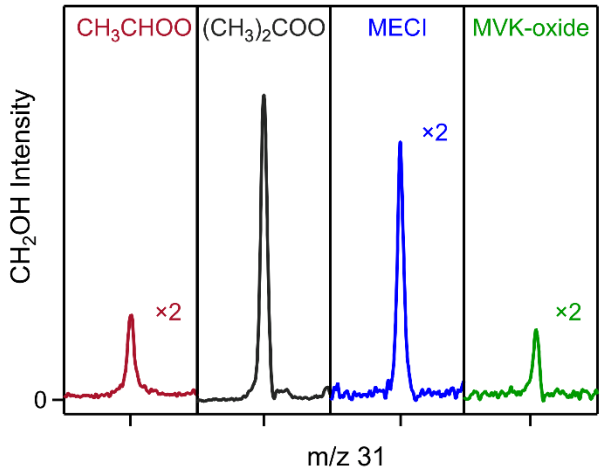

Figure 3. 2+1 REMPI signals of CH_2OH radicals (m/z 31), observed at 468.5 nm (two-photon energy of ca. 42690 cm^{-1}) upon laboratory generation of methyl-substituted Criegee intermediates, specifically CH_3CHOO, $(CH_3)_2COO$, MECI, and MVK-oxide. The CH_2OH signal intensities are scaled relative to that of the corresponding Criegee intermediate (m/z 60, 74, 88, and 86, respectively) obtained upon VUV photoionization at 118 nm.

For CH_3CHOO and MVK-oxide, the lower energy *syn*-conformers have the methyl substituent oriented toward the carbonyl oxide group, and thus can undergo 1,4 H-atom transfer leading to OH + vinoxy and potentially OH roaming (hydroxycarbonyl or CH_2OH + acyl) products. The *anti*-conformers (ca. 3 kcal mol^{-1} higher in energy) have the methyl substituent oriented away from the carbonyl oxide group and are predicted to follow different unimolecular decay pathways via dioxirane or dioxole intermediates (Scheme S1 and S2),[11, 19, 57] which do not lead to OH + vinoxy or OH roaming products. Nevertheless, the *anti*-conformers will contribute to the 10.5 eV VUV photoionization signal on m/z 60 or

m/z 86, thereby reducing the yield of OH and roaming products (including CH_2OH) relative to the Criegee intermediate (Figure 3).

The *syn*- and *anti*-conformers of the methyl-ethyl-substituted Criegee intermediate have similar ground state stabilities (within 1 kcal mol^{-1}), and are expected to be generated and detected by photoionization (m/z 88).[33, 58] The carbonyl oxide group may be oriented towards the methyl (*anti*, *E*) or ethyl (*syn*, Z) substituent. Unimolecular decay of the *anti*-MECI conformer proceeds via 1,4 H-atom transfer from the methyl ($-CH_3$) group to the terminal O-atom, which can result in O–O fission to OH radicals or OH roaming to 1-hydroxy-2-butanone [$CH_3CH_2C(O)CH_2OH$, 1H2B] and CH_2OH radicals, the latter upon C–C fission (Scheme 3). In contrast, unimolecular decay of *syn*-MECI proceeds via 1,4 H-atom transfer from the methylene ($–CH_2–$) group to the terminal O-atom, which can result in O–O fission to OH radicals, or OH roaming to 3-hydroxy-2-butanone [$CH_3CH(OH)C(O)CH_3$, 3H2B] and 1-hydroxyethyl [$CH_3CH(OH)$] radicals, the latter upon C–C fission (Scheme 3). Only *anti*-MECI can contribute to the CH_2OH signal. For *syn*-MECI, detection of 1-hydroxyethyl radicals is challenging as it requires 2+2 REMPI at ca. 564 nm via the $3p_z$ Rydberg state[59] or 2+1 REMPI at ca. 450 nm via the *4p* Rydberg state,[60] which are known to result in much weaker signals[59] and was not detected.

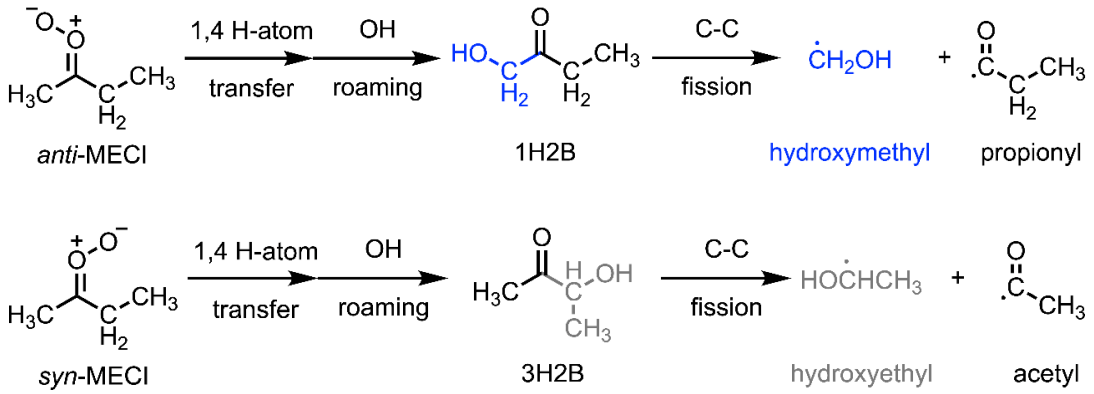

Scheme 3. Unimolecular decay of *anti*-MECI (top) via OH roaming yields 1-hydroxy-2-butanone (1H2B) with a hydroxymethyl moiety (blue), which will fragment to hydroxymethyl radicals. Analogous unimolecular decay of *syn*-MECI (bottom) yields 3-hydroxy-2-butanone (3H2B) with a 1-hydroxyethyl moiety (gray), which will fragment to 1-hydroxyethyl radicals.

B. Theoretical results

The optimized geometry of ground state CH_2OH ($X\ ^2A''$) at CASPT2/aug-cc-pVXZ (X = D, T, Q) level of theory is in good agreement with prior reports using CCSD(T)/cc-pVTZ level of theory (Table S3), the associated harmonic frequencies are listed in Table S4.[41] Analysis of the molecular orbitals reveals that the lowest four excited states are Rydberg states with *3s* ($1\ ^2A'$), $3p_x$ ($2\ ^2A'$), $3p_y$ ($3\ ^2A'$), and $3p_z$ ($2\ ^2A''$) character. Adiabatic excitation energies (AEE) are calculated for transitions to the *3p* Rydberg states (Table 1 and Table S5). The $3p_z$ Rydberg state ($2\ ^2A''$) is of particular importance in this study, as it

is involved in the 2+1 REMPI process described in the experimental results section (Figure 4). The optimized geometry and associated harmonic frequencies of $3p_z$ are given in Table S3 and Table S4. The AEE calculations in this study use the separately optimized ground and excited state geometries of CH_2OH with CASPT2 level of theory, including the zero-point energy (ZPE) correction for each state. Single-point energy corrected are then performed at the MRCI level of theory with Davidson correction, which are expected to be higher level of theory than that used in prior theoretical work.[45] The resultant values from this study are consistent with the earlier calculation results with minor discrepancy less than 0.18 eV (Table 1).

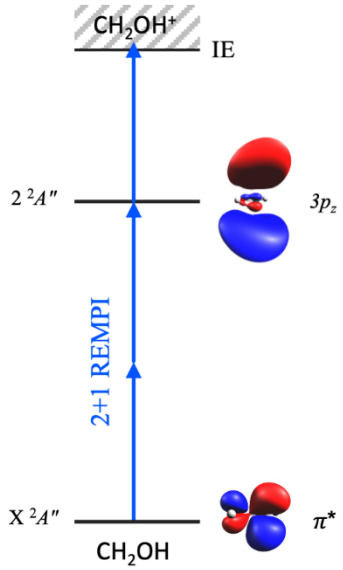

Figure 4. 2+1 REMPI scheme for CH_2OH detection via the 2 ^{2}A" electronic excited state ($3p_z$ Rydberg state), which exceeds the ionization threshold (IE) of CH_2OH.[61] The dominant orbitals (π^* and $3p_z$) involved in the two-photon transition between the X ^{2}A" and 2 ^{2}A" states are shown.

Specifically, for the $3p_z$ state, the MRCI + Q value of 5.08 eV obtained with the aug-cc-pVQZ basis set is in excellent agreement with the current experiment and previously measured[38] electronic origin of 5.09 eV with only 0.01 eV deviation. This deviation could possibly be influenced by the ΔZPE, as it was found that the rigid molecule approach is inadequate for studying the out-of-plane motions of CH_2OH.[42] The AEE values obtained at MRCI + Q level using smaller basis sets (Table S5) also qualitatively agree with the experimental results, with deviation less than 0.24 eV.

The four bands (i.e., 4_0^1, 5_0^1, 6_0^1, and 6_0^2) observed experimentally (Figure 2) are attributed to transitions from the ground state to distinct vibronic levels of the $3p_z$ Rydberg state. The calculated harmonic frequency of CH_2 scissor mode (ν_4), in-phase HCOH bending mode (ν_5), and CO stretch mode (ν_6) in the $3p_z$ state are 1499 cm^{-1}, 1419 cm^{-1} and 1661 cm^{-1}, respectively, which are ca. 30–60 cm^{-1} higher than the

experimentally observed positions of the 4_0^1, 5_0^1 and 6_0^1 bands. Nevertheless, the calculated harmonic frequencies agree with the assignment.

Table 1. Adiabatic excitation energies (AEE) computed at MRCI + Q level of theory for the electronic transition to *3p* Rydberg states in comparison with prior theoretical and experimental results.

		$3p_x \leftarrow \pi^*$	$3p_y \leftarrow \pi^*$	$3p_z \leftarrow \pi^*$
This work	MRCI+Q	4.23	4.82	5.08
	Experiment	-	-	5.09[a]
Literature	FCI[b]	4.41	4.89	5.06
	Experiment[c]	4.34	-	5.09

[a] Observed in this work at 41070 cm^{-1}.
[b] Ref. 45 calculated AEEs using the same ΔZPE = 0.14 eV for transitions to different Rydberg *3p* states, which was evaluated using the ground states of the cationic and neutral CH_2OH.
[c] Ref. 62.

Discussion

A. Energy release in OH roaming pathways

This study demonstrates that CH_2OH radicals are formed upon unimolecular decay of four different *syn*-methyl-substituted Criegee intermediates. The mechanism is illustrated in Schemes 1 and 2. The overall energetics are similar for the four systems, as shown in Figure S1. In the following discussion, we choose reference energies that correlate with the Criegee intermediates. The photolytically generated Criegee intermediates are born with a high degree of internal excitation (on the order of 50 kcal mol^{-1}), exceeding the TS barriers (16–18 kcal mol^{-1}, Table S6) for 1,4 H-atom transfer to VHPs (Table S6), which then rapidly decay. The resultant OH + vinoxy products lie higher in energy (1–8 kcal mol^{-1}, Table S6) than the Criegee intermediates, while the OH roaming channel is favored at lower energies.[23] Roaming facilitates OH addition to the vinylic CH_2-site and yields hydroxycarbonyl products within a deep potential well with stability of 82 to 87 kcal mol^{-1} (Table S7).

Under limited collision conditions, the energized hydroxycarbonyls formed via roaming may dissociate by C–C bond fission and yield CH_2OH + acyl radical products, which again lie lower in energy than the Criegee intermediates (by 1–5 kcal mol^{-1}, Table S7). The resultant CH_2OH radicals are formed with substantial internal excitation. We calculate the average vibrational energy of the CH_2OH radicals using statistical partitioning of the total energy (E_{tot}) available to the CH_2OH + acyl radical pair, as follows:

$$\langle E, E_{tot} \rangle = \frac{\int_0^{E_{tot}} E\, \rho(E)\, G(E_{tot}-E)\, dE}{\int_0^{E_{tot}} \rho(E)\, G(E_{tot}-E)\, dE}$$

Here, ρ is the density of states of the CH_2OH radical, G is the sum of states of the acyl radical coproduct, E_{tot} combines the initial internal energy of the Criegee intermediate with the exothermicity associated with the Criegee intermediate channel to C–C fission products (Table S7), and E is the energy flowing to CH_2OH. This approach has been previously used to obtain the energy distribution of the Criegee intermediate upon dissociation of the primary ozonide in alkene ozonolysis.[63, 64] We calculate the sums and densities of states using the DENSUM function of the MULTIWELL program suite[65, 66] with harmonic frequencies obtained at the CCSD(T)/cc-pVTZ level of theory.

As shown in Figure 5, as the size of the acyl coproduct increases, less internal excitation of CH_2OH is expected. For example, fragmentation of glycolaldehyde (from CH_3CHOO) gives rise to CH_2OH (five-atom) and formyl (three-atom) radical products. CH_2OH has more vibrational modes than formyl and, as a result, more than half of E_{tot} will be distributed to CH_2OH upon C–C fission. Representative vibrational energy distributions of the CH_2OH radicals are shown in Figure S6, when the corresponding Criegee intermediates have 50 kcal mol^{-1} of internal energy. Specifically, ca. 37 kcal mol^{-1} on average will be partitioned to CH_2OH when CH_3CHOO has 50 kcal mol^{-1} of internal energy. Collisional relaxation of the nascent CH_3CHOO within the capillary tube will result in lower vibrational excitation of CH_2OH. A portion of the newly formed CH_2OH is expected to have sufficiently high internal energy to undergo C–H bond breakage (dissociation energy of 29 kcal mol^{-1}) and form H-atom + formaldehyde products.[67, 68] Such secondary dissociation will lead to reduced CH_2OH yield in the CH_3CHOO system. For the other larger hydroxycarbonyls, an average of ca. 14–20 kcal mol^{-1} will be partitioned into CH_2OH if the corresponding Criegee intermediates [$(CH_3)_2COO$, *anti*-MECI, and *syn*-MVK-oxide] have 50 kcal mol^{-1} of internal energy. Again, collisional relaxation of these Criegee intermediates will reduce the amount of energy available to CH_2OH products; as a result, dissociative loss of CH_2OH is not expected to be significant in these systems. Also, reactive loss of CH_2OH with O_2 is not included due to limited reaction time within the capillary tube (μs).[69, 70] The CH_2OH radicals are then cooled in the free jet expansion prior to 2+1 REMPI detection. Other possible decay pathways of hydroxycarbonyls, including H_2 elimination forming dicarbonyl,[26] C–OH bond breakage forming OH + vinoxy,[26] intramolecular H-abstraction during C–C fission to form multiple close-shell products,[23] and/or secondary dissociation of acyl radicals,[71] are not explored in this study.

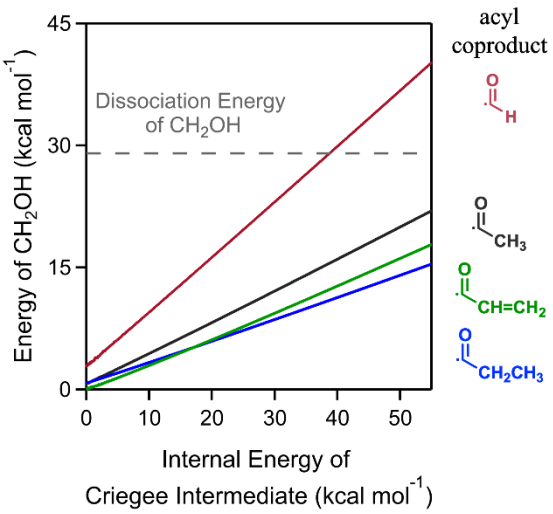

Figure 5. The average vibrational energy partitioned into CH_2OH upon C–C fission of the hydroxycarbonyl following the unimolecular decay of *syn*-CH_3CHOO (red), $(CH_3)_2COO$ (black), *anti*-MECI (blue), and *syn*-MVK-oxide (green) with different amounts of initial internal excitation. The gray dashed line indicates the energy required for secondary dissociation of the hydroxymethyl radical to H-atom + formaldehyde from Ref. 68.

B. CH_2OH radical yield

The largest signal intensity for CH_2OH (relative to corresponding Criegee intermediate; Figure 3) have been observed following unimolecular decay of $(CH_3)_2COO$. For unimolecular decay of MECI, the CH_2OH signal intensity is approximately half of that observed for $(CH_3)_2COO$. This change may originate from their different conformer distributions: $(CH_3)_2COO$ has only a single conformational form, while MECI has *anti*- and *syn*-conformers (within 1 kcal mol^{-1}). The *anti*/*syn* isomerization involves rotation about C=O double bond and is associated with a barrier of ca. 37 kcal mol^{-1}.[11] Newly formed MECI (with ca. 50 kcal mol^{-1} internal energy) is expected to populate both configurations, but interconversion will become restricted upon collisional relaxation. Equal population is assumed for collisionally stabilized *anti*- and *syn*-MECI.[18] However, only *anti*-MECI (ca. half of the total MECI) can yield CH_2OH via OH roaming, resulting in half the CH_2OH yield compared to $(CH_3)_2COO$. Importantly, a recent theoretical study on MECI has shown that roaming is only significant at low energies (ca. 5 kcal mol^{-1}) relative to the OH + vinoxy asymptote, and thus roaming will not be relevant until the system is significantly relaxed.[23] Taking into account the conformer distribution of MECI, it appears that the probability of OH roaming is similar for *anti*-MECI and $(CH_3)_2COO$. A plausible explanation is their structural similarity as doubly-alkyl-substituted Criegee intermediates and comparable energetics along the reaction coordinates (Tables S6 and S7).

For CH_3CHOO, only the lower-energy *syn*-conformer can undergo 1,4 H-atom transfer and subsequent VHP decay, leading to OH radical or roaming products. *Syn*-CH_3CHOO has been previously

reported as the predominant conformer, with an estimated population fraction of 70–90%.[72-75] However, the CH_2OH signal intensity from CH_3CHOO in the present experiments is much smaller than observed for $(CH_3)_2COO$ (Figure 3). The smaller CH_2OH yield for CH_3CHOO may be indicative of less roaming, as shown in simulations under thermal conditions,[22] and/or secondary dissociation of CH_2OH (Figure 5).[67, 68] Additional factors that may impact the yield of CH_2OH radicals include collisional stabilization of the hydroxycarbonyl and/or bimolecular reaction of CH_2OH with O_2. Observation of CH_2OH is the first direct experimental evidence of roaming for CH_3CHOO.

In the case of MVK-oxide,[34] OH radicals will primarily result from unimolecular decay of internally excited *syn*-MVK-oxide, involving H-atom transfer from the methyl group and subsequent dissociation of VHP; the alternative roaming pathway will lead to CH_2OH products. Energized *anti*-MVK-oxide is expected to decay via a low-barrier 1,5 ring-closure pathway to dioxole (Scheme S2, TS barrier of 12 kcal mol^{-1}),[19, 57] which will not yield OH or CH_2OH products. The CH_2OH signal intensity is ca. 1/3 of that for MECI (Figure 3). While roaming appears to be less favorable in the unimolecular decay of *syn*-MVK-oxide, the appearance of CH_2OH is the first experimental observation of roaming for this isoprene-derived Criegee intermediate, validating a prior theoretical prediction.[19]

Under atmospheric conditions, we anticipate that roaming in the unimolecular decay of *syn*-methyl-substituted Criegee intermediates will primarily yield hydroxycarbonyls, rather than the CH_2OH radicals observed under the limited-collision conditions in this work. The predominant atmospheric removal pathways of hydroxycarbonyls are bimolecular reaction with OH radicals and a minor photolytic loss channel. For example, the UV absorption spectrum of hydroxyacetone peaks at 266 nm with maximum absorption cross-section of 6.7×10^{-20} cm^2 $molecule^{-1}$, leading to an estimated photolysis lifetime of 2 weeks.[76] OH radicals can initiate oxidation of hydroxyacetone by H-atom abstraction from the $-CH_2-$ site, which is followed by O_2 addition and HO_2 elimination, yielding methylglyoxal [$CH_3C(O)CHO$] as the primary product (> 90%).[76] The bimolecular reaction rate coefficient with OH was reported to be 3.0×10^{-12} cm^3 $molecule^{-1}$ s^{-1}, limiting the tropospheric lifetime of hydroxyacetone to four days assuming an average OH concentration of 10^6 molecule cm^{-3}.[76, 77] As a general result, hydroxycarbonyls from roaming will be oxidized into dicarbonyls by sequential reaction with OH and O_2 in the atmosphere. Dicarbonyls are more reactive than hydroxycarbonyls and have been reported as a source of secondary organic aerosol.[78, 79]

Conclusions

Syn-methyl-substituted Criegee intermediates generated in a capillary reactor tube undergo unimolecular decay via 1,4 H-atom transfer, transiently forming vinyl hydroperoxide intermediates, which dissociate to OH + vinoxy radical products or, alternatively, isomerize to hydroxycarbonyl products

via OH roaming. For four *syn*-methyl-substituted Criegee intermediates, unimolecular decay has been shown to yield hydroxycarbonyl products with sufficient internal energy to dissociate via C–C fission to acyl and CH_2OH radicals. The CH_2OH product has been identified upon supersonic expansion by 2+1 REMPI detection via the $3p_z$ Rydberg state on the m/z 31 mass channel. The adiabatic excitation energy associated with the electronic transition from the ground state to the $3p_z$ Rydberg state of CH_2OH is calculated with high-level ab initio methods, which shows good agreement with experiment. In addition, the stabilized Criegee intermediates are separately detected under similar experimental conditions using VUV (118 nm) photoionization.

The probability of roaming appears to be similar for unimolecular decay of $(CH_3)_2COO$ and *anti*-MECI, and seems to be lower for *syn*-CH_3CHOO and *syn*-MVK-oxide. Nevertheless, this study provides the first experimental evidence of roaming for *syn*-MVK-oxide, an isoprene-derived Criegee intermediate, confirming a prior theoretical prediction,[19] which also predicted C–C fission of the hydroxycarbonyl under collision-free or limited collision conditions. Prior studies of $(CH_3)_2COO$ and MECI under thermal conditions identified hydroxyacetone and hydroxybutanone, products,[21, 23] respectively, while this study reveals CH_2OH radicals resulting from C–C fragmentation of the hydroxycarbonyls. This study demonstrates that OH roaming will commonly occur in the unimolecular decay of *syn*-methyl-substituted Criegee intermediates, although the dominant decay channel yields OH + vinoxy radical products.

Supporting Information Description

The Supporting Information contains schemes and tables related to unimolecular decay mechanisms and energetics, analysis of rotational and vibrational cooling of CH_2OH, additional mass spectrometry data and REMPI spectra, and electronic structure calculations for CH_2OH.

Acknowledgments

Research supported by the National Science Foundation under grants CHE-1955068 and CHE-2301298. This work used the Advanced Cyberinfrastructure Coordination Ecosystem: Service & Support (ACCESS) program, which is supported by National Science Foundation grants #2138259, #2138286, #2138307, #2137603, and #2138296, through the allocation TG-CHE190088. The authors thank Stephen J. Klippenstein (Argonne) for helpful discussions.

References

(1) Gligorovski, S.; Strekowski, R.; Barbati, S.; Vione, D. Environmental Implications of Hydroxyl Radicals (•OH). *Chem. Rev.* **2015**, *115* (24), 13051-13092. DOI: 10.1021/cr500310b.

(2) Atkinson, R. Kinetics and Mechanisms of the Gas-Phase Reactions of the Hydroxyl Radical with Organic-Compounds under Atmospheric Conditions. *Chem. Rev.* **1986**, *86* (1), 69-201. DOI: 10.1021/cr00071a004.

(3) Emmerson, K. M.; Carslaw, N. Night-time radical chemistry during the TORCH campaign. *Atmos. Environ.* **2009**, *43* (20), 3220-3226. DOI: 10.1016/j.atmosenv.2009.03.042.

(4) Emmerson, K. M.; Carslaw, N.; Carslaw, D. C.; Lee, J. D.; McFiggans, G.; Bloss, W. J.; Gravestock, T.; Heard, D. E.; Hopkins, J.; Ingham, T.; et al. Free radical modelling studies during the UK TORCH Campaign in Summer 2003. *Atmos. Chem. Phys.* **2007**, *7*, 167-181. DOI: 10.5194/acp-7-167-2007.

(5) Harrison, R. M.; Yin, J.; Tilling, R. M.; Cai, X.; Seakins, P. W.; Hopkins, J. R.; Lansley, D. L.; Lewis, A. C.; Hunter, M. C.; Heard, D. E.; et al. Measurement and modelling of air pollution and atmospheric chemistry in the UK West Midlands conurbation: Overview of the PUMA Consortium project. *Sci. Total Environ.* **2006**, *360* (1-3), 5-25. DOI: 10.1016/j.scitotenv.2005.08.053.

(6) Elshorbany, Y. F.; Kurtenbach, R.; Wiesen, P.; Lissi, E.; Rubio, M.; Villena, G.; Gramsch, E.; Rickard, A. R.; Pilling, M. J.; Kleffmann, J. Oxidation capacity of the city air of Santiago, Chile. *Atmos. Chem. Phys.* **2009**, *9* (6), 2257-2273. DOI: 10.5194/acp-9-2257-2009.

(7) Osborn, D. L.; Taatjes, C. A. The physical chemistry of Criegee intermediates in the gas phase. *Int. Rev. Phys. Chem.* **2015**, *34* (3), 309-360. DOI: 10.1080/0144235x.2015.1055676.

(8) Taatjes, C. A.; Shallcross, D. E.; Percival, C. J. Research frontiers in the chemistry of Criegee intermediates and tropospheric ozonolysis. *Phys. Chem. Chem. Phys.* **2014**, *16* (5), 1704-1718. DOI: 10.1039/c3cp52842a.

(9) Lester, M. I.; Klippenstein, S. J. Unimolecular Decay of Criegee Intermediates to OH Radical Products: Prompt and Thermal Decay Processes. *Acc. Chem. Res.* **2018**, *51* (4), 978-985. DOI: 10.1021/acs.accounts.8b00077.

(10) Mauldin, R. L.; Berndt, T.; Sipila, M.; Paasonen, P.; Petaja, T.; Kim, S.; Kurten, T.; Stratmann, F.; Kerminen, V. M.; Kulmala, M. A new atmospherically relevant oxidant of sulphur dioxide. *Nature* **2012**, *488* (7410), 193-196. DOI: 10.1038/nature11278.

(11) Vereecken, L.; Novelli, A.; Taraborrelli, D. Unimolecular decay strongly limits the atmospheric impact of Criegee intermediates. *Phys. Chem. Chem. Phys.* **2017**, *19* (47), 31599-31612. DOI: 10.1039/c7cp05541b.

(12) Vereecken, L.; Harder, H.; Novelli, A. The reaction of Criegee intermediates with NO, RO_2, and SO_2, and their fate in the atmosphere. *Phys. Chem. Chem. Phys.* **2012**, *14* (42), 14682-14695. DOI: 10.1039/c2cp42300f.

(13) Fang, Y.; Barber, V. P.; Klippenstein, S. J.; Mccoy, A. B.; Lester, M. I. Tunneling effects in the unimolecular decay of $(CH_3)_2COO$ Criegee intermediates to OH radical products. *J. Chem. Phys.* **2017**, *146* (13), 134307. DOI: 10.1063/1.4979297.

(14) Fang, Y.; Liu, F.; Barber, V. P.; Klippenstein, S. J.; McCoy, A. B.; Lester, M. I. Communication: Real time observation of unimolecular decay of Criegee intermediates to OH radical products. *J. Chem. Phys.* **2016**, *144* (6), 061102. DOI: 10.1063/1.4941768.

(15) Fang, Y.; Liu, F.; Barber, V. P.; Klippenstein, S. J.; McCoy, A. B.; Lester, M. I. Deep tunneling in the unimolecular decay of CH_3CHOO Criegee intermediates to OH radical products. *J. Chem. Phys.* **2016**, *145* (23), 234308. DOI: 10.1063/1.4972015.

(16) Fang, Y.; Liu, F.; Klippenstein, S. J.; Lester, M. I. Direct observation of unimolecular decay of CH_3CH_2CHOO Criegee intermediates to OH radical products. *J. Chem. Phys.* **2016**, *145* (4), 044312. DOI: 10.1063/1.4958992.

(17) Liu, F.; Beames, J. M.; Petit, A. S.; McCoy, A. B.; Lester, M. I. Infrared-driven unimolecular reaction of CH_3CHOO Criegee intermediates to OH radical products. *Science* **2014**, *345* (6204), 1596-1598. DOI: 10.1126/science.1257158.

(18) Barber, V. P.; Hansen, A. S.; Georgievskii, Y.; Klippenstein, S. J.; Lester, M. I. Experimental and theoretical studies of the doubly substituted methyl-ethyl Criegee intermediate: Infrared action spectroscopy and unimolecular decay to OH radical products. *J. Chem. Phys.* **2020**, *152* (9), 094301. DOI: 10.1063/5.0002422.
(19) Barber, V. P.; Pandit, S.; Green, A. M.; Trongsiriwat, N.; Wash, P. J.; Klippenstein, S. J.; Lester, M. I. Four-Carbon Criegee Intermediate from Isoprene Ozonolysis: Methyl Vinyl Ketone Oxide Synthesis, Infrared Spectrum, and OH Production. *J. Am. Chem. Soc.* **2018**, *140* (34), 10866-10880. DOI: 10.1021/jacs.8b06010.
(20) Stephenson, T. A.; Lester, M. I. Unimolecular decay dynamics of Criegee intermediates: Energy-resolved rates, thermal rates, and their atmospheric impact. *Int. Rev. Phys. Chem.* **2020**, *39* (1), 1-33. DOI: 10.1080/0144235X.2020.1688530.
(21) Taatjes, C. A.; Liu, F.; Rotavera, B.; Kumar, M.; Caravan, R.; Osborn, D. L.; Thompson, W. H.; Lester, M. I. Hydroxyacetone Production From C3 Criegee Intermediates. *J. Phys. Chem. A* **2017**, *121* (1), 16-23. DOI: 10.1021/acs.jpca.6b07712.
(22) Kuwata, K. T.; Luu, L. N.; Weberg, A. B.; Huang, K.; Parsons, A. J.; Peebles, L. A.; Rackstraw, N. B.; Kim, M. J. Quantum Chemical and Statistical Rate Theory Studies of the Vinyl Hydroperoxides Formed in *trans*-2-Butene and 2,3-Dimethyl-2-butene Ozonolysis. *J. Phys. Chem. A* **2018**, *122* (9), 2485-2502. DOI: 10.1021/acs.jpca.8b00287.
(23) Liu, T.; Elliot, S. N.; Zou, M.; Vansco, M. F.; Sojdak, C. A.; Markus, C. R.; Almeida, R.; Au, K.; Sheps, L.; Osborn, D. L.; et al. OH Roaming and Beyond in the Unimolecular Decay of the Methyl-Ethyl Substituted Criegee Intermediate: Observations and Predictions. *J. Am. Chem. Soc.* **2023**, *145* (35), 19405-19420. DOI: 10.1021/jacs.3c07126.
(24) Klippenstein, S. J.; Elliott, S. N. OH Roaming During the Ozonolysis of α-Pinene: A New Route to Highly Oxygenated Molecules? *J. Phys. Chem.* **2023**, *submitted*.
(25) Niki, H.; Maker, P. D.; Savage, C. M.; Breitenbach, L. P.; Hurley, M. D. FTIR Spectroscopic Study of the Mechanism for the Gas-Phase Reaction between Ozone and Tetramethylethylene. *J. Phys. Chem.* **1987**, *91* (4), 941-946. DOI: 10.1021/j100288a035.
(26) Grosjean, D.; Grosjean, E.; Williams, E. L. Atmospheric Chemistry of Olefins: a Product Study of the Ozone Alkene Reaction with Cyclohexane Added to Scavenge OH. *Environ. Sci. Technol.* **1994**, *28* (1), 186-196. DOI: 10.1021/es00050a026.
(27) Conrad, A. R.; Hansen, N.; Jasper, A. W.; Thomason, N. K.; Hidaldo-Rodrigues, L.; Treshock, S. P.; Popolan-Vaida, D. M. Identification of the acetaldehyde oxide Criegee intermediate reaction network in the ozone-assisted low-temperature oxidation of *trans*-2-butene. *Phys. Chem. Chem. Phys.* **2021**, *23* (41), 23554-23566. DOI: 10.1039/d1cp03126k.
(28) Kalalian, C.; Roth, E.; El Dib, G.; Singh, H. J.; Rao, P. K.; Chakir, A. Product investigation of the gas phase ozonolysis of 1-penten-3-ol, *cis*-2-penten-1-ol and *trans*-3-hexen-1-ol. *Atmos. Environ.* **2020**, *238*, 117732. DOI: 10.1016/j.atmosenv.2020.117732.
(29) Welz, O.; Savee, J. D.; Osborn, D. L.; Vasu, S. S.; Percival, C. J.; Shallcross, D. E.; Taatjes, C. A. Direct Kinetic Measurements of Criegee Intermediate (CH_2OO) Formed by Reaction of CH_2I with O_2. *Science* **2012**, *335* (6065), 204-207. DOI: 10.1126/science.1213229.
(30) Barber, V. P.; Pandit, S.; Esposito, V. J.; McCoy, A. B.; Lester, M. I. CH Stretch Activation of CH_3CHOO: Deep Tunneling to Hydroxyl Radical Products. *J. Phys. Chem. A* **2019**, *123* (13), 2559-2569. DOI: 10.1021/acs.jpca.8b12324.
(31) Beames, J. M.; Liu, F.; Lu, L.; Lester, M. I. UV spectroscopic characterization of an alkyl substituted Criegee intermediate CH_3CHOO. *J. Chem. Phys.* **2013**, *138* (24), 244307. DOI: 10.1063/1.4810865.
(32) Liu, F.; Beames, J. M.; Green, A. M.; Lester, M. I. UV Spectroscopic Characterization of Dimethyl- and Ethyl-Substituted Carbonyl Oxides. *J. Phys. Chem. A* **2014**, *118* (12), 2298-2306. DOI: 10.1021/jp412726z.
(33) Liu, T.; Zou, M.; Caracciolo, A.; Sojdak, C. A.; Lester, M. I. Substituent effects on the electronic spectroscopy of four-carbon Criegee intermediates. *J. Phys. Chem. A* **2022**, *126* (38), 6734-6741.

(34) Vansco, M. F.; Marchetti, B.; Lester, M. I. Electronic spectroscopy of methyl vinyl ketone oxide: A four-carbon unsaturated Criegee intermediate from isoprene ozonolysis. *J. Chem. Phys.* **2018**, *149* (24), 244309. DOI: 10.1063/1.5064716.
(35) Barber, V. P.; Esposito, V. J.; Trabelsi, T.; Hansen, A. S.; McHenry, T. A.; Francisco, J. S.; Lester, M. I. Experimental and computational investigation of vinoxy and 1-methylvinoxy radicals from the unimolecular decay of alkyl-substituted Criegee intermediates. *Chem. Phys. Lett.* **2020**, *751*, 137478. DOI: 10.1016/j.cplett.2020.137478.
(36) Dulcey, C. S.; Hudgens, J. W. Multiphoton Ionization Spectroscopy and Vibrational Analysis of a 3p Rydberg State of the Hydroxymethyl Radical. *J. Chem. Phys.* **1986**, *84* (10), 5262-5270. DOI: 10.1063/1.449935.
(37) Dulcey, C. S.; Hudgens, J. W. Detection of CH_2OH Radicals by Resonance-Enhanced Multiphoton Ionization Spectroscopy. *J. Phys. Chem.* **1983**, *87* (13), 2296-2298. DOI: 10.1021/j100236a012.
(38) Aristov, V.; Conroy, D.; Reisler, H. Symmetry and Lifetime of the hydroxymethyl radical in the 3p Rydberg state. *Chem. Phys. Lett.* **2000**, *318* (4-5), 393-401. DOI: 10.1016/S0009-2614(00)00042-7.
(39) Rettrup, S.; Pagsberg, P.; Anastasi, C. Ab initio Configuration-Interaction Study of the Rydberg States of the Hydroxymethyl Radical CH_2OH. *Chem. Phys. Lett.* **1988**, *122* (1), 45-51. DOI: 10.1016/0301-0104(88)87258-6.
(40) Conroy, D.; Aristov, V.; Feng, L.; Reisler, H. Predissociation of the hydroxymethyl radical in the $3p_z$ Rydberg state: Formaldehyde plus hydrogen atom channel. *J. Phys. Chem. A* **2000**, *104* (45), 10288-10292. DOI: 10.1021/jp001357s.
(41) Karpichev, B.; Reisler, H.; Krylov, A. I.; Diri, K. Effect of hyperconjugation on ionization energies of hydroxyalkyl radicals. *J. Phys. Chem. A* **2008**, *112* (40), 9965-9969. DOI: 10.1021/jp805250t.
(42) Marenich, A. V.; Boggs, J. E. A variational study of nuclear dynamics and structural flexibility of the CH_2OH radical. *J. Chem. Phys.* **2003**, *119* (6), 3098-3105. DOI: 10.1063/1.1591730.
(43) Marenich, A. V.; Boggs, J. E. Structural and thermochemical properties of the hydroxymethyl (CH_2OH) radical: A high precision ab initio study. *J. Chem. Phys.* **2003**, *119* (19), 10105-10114. DOI: 10.1063/1.1618736.
(44) Chen, F. W.; Davidson, E. R. Theoretical study of the electronic spectrum and ESR of the CH_2OH radical. *J. Phys. Chem. A* **2001**, *105* (18), 4558-4562. DOI: 10.1021/jp004458z.
(45) Bruna, P. J.; Grein, F. The electronic spectrum of H_2COH revisited. *J. Phys. Chem. A* **2001**, *105* (37), 8599-8603. DOI: 10.1021/jp012385t.
(46) Roth, A. *Vacuum technology*; Elsevier North-Holland, INC., 1982.
(47) Konen, I. M.; Pollack, I. B.; Li, E. X. J.; Lester, M. I.; Varner, M. E.; Stanton, J. F. Infrared overtone spectroscopy and unimolecular decay dynamics of peroxynitrous acid. *J. Chem. Phys.* **2005**, *122* (9), 094320. DOI: 10.1063/1.1854094.
(48) *MOLPRO, version 2020.1, A Package of Ab Initio Programs; see http://www.molpro.net.*; (accessed March 2023).
(49) Werner, H. J.; Knowles, P. J.; Manby, F. R.; Black, J. A.; Doll, K.; Hesselmann, A.; Kats, D.; Kohn, A.; Korona, T.; Kreplin, D. A.; et al. The Molpro quantum chemistry package. *J. Chem. Phys.* **2020**, *152* (14), 144107. DOI: 10.1063/5.0005081.
(50) Lehman, J. H.; Li, H. W.; Lester, M. I. Ion imaging studies of the photodissociation dynamics of CH_2I_2 at 248 nm. *Chem. Phys. Lett.* **2013**, *590*, 16-21. DOI: 10.1016/j.cplett.2013.10.029.
(51) Toulson, B. W.; Alaniz, J. P.; Hill, J. G.; Murray, C. Near-UV photodissociation dynamics of CH_2I_2. *Phys. Chem. Chem. Phys.* **2016**, *18* (16), 11091-11103. DOI: 10.1039/c6cp01063f.
(52) Cai, J. R.; Su, J. H.; Lee, Y. P. Formation reaction mechanism and infrared spectra of anti-trans-methacrolein oxide and its associated precursor and adduct radicals. *Commun. Chem.* **2022**, *5* (1), 26. DOI: 10.1038/s42004-022-00644-0.
(53) Huang, Y. H.; Chen, L. W.; Lee, Y. P. Simultaneous Infrared Detection of the ICH_2OO Radical and Criegee Intermediate CH_2OO: The Pressure Dependence of the Yield of CH_2OO in the Reaction $CH_2I + O_2$. *J. Phys. Chem. Lett.* **2015**, *6* (22), 4610-4615. DOI: 10.1021/acs.jpclett.5b02298.

(54) Lin, Y. H.; Li, Y. L.; Chao, W.; Takahashi, K.; Lin, J. J. M. The role of the iodine-atom adduct in the synthesis and kinetics of methyl vinyl ketone oxide-a resonance-stabilized Criegee intermediate. *Phys. Chem. Chem. Phys.* **2020**, *22* (24), 13603-13612. DOI: 10.1039/d0cp02085k.
(55) Conroy, D. G. Rydberg state of an open shell species: Characterization and photophysics of the 3p (z) state of hydroxymethyl radical. Ph.D. Thesis. University of Southern California, 2000.
(56) Kidwell, N. M.; Li, H. W.; Wang, X. H.; Bowman, J. M.; Lester, M. I. Unimolecular dissociation dynamics of vibrationally activated CH_3CHOO Criegee intermediates to OH radical products. *Nat. Chem.* **2016**, *8* (5), 509-514. DOI: 10.1038/Nchem.2488.
(57) Vansco, M. F.; Caravan, R. L.; Zuraski, K.; Winiberg, F. A. F.; Au, K.; Trongsiriwat, N.; Walsh, P. J.; Osborn, D. L.; Percival, C. J.; Khan, M. A. H.; et al. Experimental Evidence of Dioxole Unimolecular Decay Pathway for Isoprene-Derived Criegee Intermediates. *J. Phys. Chem. A* **2020**, *124* (18), 3542-3554. DOI: 10.1021/acs.jpca.0c02138.
(58) Cabezas, C.; Guillemin, J. C.; Endo, Y. Probing the conformational behavior of the doubly substituted methyl-ethyl Criegee intermediate by FTMW spectroscopy. *J. Chem. Phys.* **2017**, *146* (17), 174304. DOI: 10.1063/1.4982682.
(59) Karpichev, B.; Edwards, L. W.; Wei, J.; Reisler, H. Electronic spectroscopy and photodissociation dynamics of the 1-hydroxyethyl radical CH_3CHOH. *J. Phys. Chem. A* **2008**, *112* (3), 412-418. DOI: 10.1021/jp077213w.
(60) Edelbüttel-Einhaus, J.; Hoyermann, K.; Rohde, G.; Seeba, J. The detection of the hydroxyethyl radical by REMPI/mass-spectrometry and the application to the study of the reactions CH_3CHOH+ O and CH_3CHOH+ H. In *Proceedings of the 24th Symposium International on Combustion; Combustion Institute: Pittsburgh, PA*, 1992; Elsevier: Vol. 24, pp 661-668.
(61) Lias, S. G. "Ionization Energy Evaluation" in NIST Chemistry WebBook, NIST Standard Reference Database Number 69, Eds. P.J. Linstrom and W.G. Mallard, National Institute of Standards and Technology, Gaithersburg MD, 20899, https://doi.org/10.18434/T4D303, (retrieved April 10, 2023).
(62) Edwards, L. W. Spectroscopy and photodissociation dynamics of hydroxyethyl radicals. Ph.D. Thesis. University of Southern California, 2010.
(63) Drozd, G. T.; Kurten, T.; Donahue, N. M.; Lester, M. I. Unimolecular Decay of the Dimethyl-Substituted Criegee Intermediate in Alkene Ozonolysis: Decay Time Scales and the Importance of Tunneling. *J. Phys. Chem. A* **2017**, *121* (32), 6036-6045. DOI: 10.1021/acs.jpca.7b05495.
(64) Kroll, J. H.; Sahay, S. R.; Anderson, J. G.; Demerjian, K. L.; Donahue, N. M. Mechanism of HOx formation in the gas-phase ozone-alkene reaction. 2. Prompt versus thermal dissociation of carbonyl oxides to form OH. *J. Phys. Chem. A* **2001**, *105* (18), 4446-4457. DOI: 10.1021/jp004136v.
(65) Barker, J. R. Multiple-well, multiple-path unimolecular reaction systems. I. MultiWell computer program suite. *Int. J. Chem. Kinet.* **2001**, *33* (4), 232-245. DOI: 10.1002/kin.1017.
(66) Barker, J. R.; Nguyen, T. L.; Stanton, J. F.; Aieta, C.; Ceotto, M.; Gabas, F.; Kumar, T. J. D.; Li, C. G. L.; Lohr, L. L.; Maranzana, A.; et al. MultiWell-2021 Software Suite; University of Michigan, Ann Arbor, Michigan, USA, Jan 2021; https://multiwell.engin.umich.edu (accessed July 2023).
(67) Ryazanov, M.; Rodrigo, C.; Reisler, H. Overtone-induced dissociation and isomerization dynamics of the hydroxymethyl radical (CH_2OH and CD_2OH). I. A theoretical study. *J. Chem. Phys.* **2012**, *136* (8), 084304. DOI: 10.1063/1.3685899.
(68) Ryazanov, M.; Rodrigo, C.; Reisler, H. Overtone-induced dissociation and isomerization dynamics of the hydroxymethyl radical (CH_2OH and CD_2OH). II. Velocity map imaging studies. *J. Chem. Phys.* **2012**, *136* (8), 084305. DOI: 10.1063/1.3685899.
(69) Miyoshi, A.; Matsui, H.; Washida, N. Rates of Reaction of Hydroxyalkyl Radicals with Molecular-Oxygen. *J. Phys. Chem.* **1990**, *94* (7), 3016-3019. DOI: 10.1021/j100370a052.
(70) Schocker, A.; Uetake, M.; Kanno, N.; Koshi, M.; Tonokura, K. Kinetics and rate constants of the reaction CH_2OH+O_2 -> CH_2O+HO_2 in the temperature range of 236-600 K. *J. Phys. Chem. A* **2007**, *111* (29), 6622-6627. DOI: 10.1021/jp0682513.
(71) Wu, Y.; Xie, D. Q.; Xue, Y. Ab initio studies for the photodissociation mechanism of hydroxyacetone. *J. Comput. Chem.* **2003**, *24* (8), 931-938. DOI: 10.1002/jcc.10264.

(72) Taatjes, C. A.; Welz, O.; Eskola, A. J.; Savee, J. D.; Scheer, A. M.; Shallcross, D. E.; Rotavera, B.; Lee, E. P. F.; Dyke, J. M.; Mok, D. K. W.; et al. Direct Measurements of Conformer-Dependent Reactivity of the Criegee Intermediate CH_3CHOO. *Science* **2013**, *340* (6129), 177-180. DOI: 10.1126/science.1234689.
(73) Sheps, L.; Scully, A. M.; Au, K. UV absorption probing of the conformer-dependent reactivity of a Criegee intermediate CH_3CHOO. *Phys. Chem. Chem. Phys.* **2014**, *16* (48), 26701-26706. DOI: 10.1039/c4cp04408h.
(74) Nakajima, M.; Endo, Y. Communication: Spectroscopic characterization of an alkyl substituted Criegee intermediate *syn*-CH_3CHOO through pure rotational transitions. *J. Chem. Phys.* **2014**, *140* (1), 011101. DOI: 10.1063/1.4861494.
(75) Lin, H. Y.; Huang, Y. H.; Wang, X. H.; Bowman, J. M.; Nishimura, Y.; Witek, H. A.; Lee, Y. P. Infrared identification of the Criegee intermediates *syn*- and *anti*-CH_3CHOO, and their distinct conformation-dependent reactivity. *Nat. Commun.* **2015**, *6* (1), 7012. DOI: 10.1038/ncomms8012.
(76) Orlando, J. J.; Tyndall, G. S.; Fracheboud, J. M.; Estupinan, E. G.; Haberkorn, S.; Zimmer, A. The rate and mechanism of the gas-phase oxidation of hydroxyacetone. *Atmos. Environ.* **1999**, *33* (10), 1621-1629. DOI: 10.1016/S1352-2310(98)00386-0.
(77) Dagaut, P.; Liu, R. Z.; Wallington, T. J.; Kurylo, M. J. Kinetic Measurements of the Gas-Phase Reactions of Oh Radicals with Hydroxy Ethers, Hydroxy Ketones, and Keto Ethers. *J. Phys. Chem.* **1989**, *93* (23), 7838-7840. DOI: 10.1021/j100360a022.
(78) Wang, S. Y.; Du, L.; Tsona, N. T.; Jiang, X. T.; You, B.; Xu, L.; Yang, Z. M.; Wang, W. X. Effect of NOx and SO_2 on the photooxidation of methylglyoxal: Implications in secondary aerosol formation. *J. Environ. Sci.* **2020**, *92*, 151-162. DOI: 10.1016/j.jes.2020.02.011.
(79) Fu, T. M.; Jacob, D. J.; Wittrock, F.; Burrows, J. P.; Vrekoussis, M.; Henze, D. K. Global budgets of atmospheric glyoxal and methylglyoxal, and implications for formation of secondary organic aerosols. *J. Geophys. Res.* **2008**, *113*, D15303. DOI: 10.1029/2007jd009505.

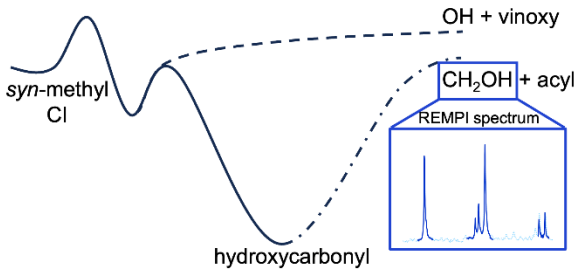
OH + vinoxy
syn-methyl
Cl
CH2OH + acyl
REMPI spectrum
hydroxycarbonyl

TOC figure